Journal of Marine Science and Technology

Volume 27 | Issue 6 Article 1

DYNAMIC RESPONSE ANALYSIS OF THE LIFTING LOAD SYSTEM OF A CRANE SHIP IN IRREGULAR WAVES

Xiao-Rong Yang
Military Transportation University, Tianjin 300161, China. Tianjin University Renai College, Tianjin 301636, China, Luaiyxr@163.com

Qiu-Ming Gan
Military Transportation Research Institute, Tianjin 300161, China

Yan-Hong Wang
Military Transportation University, Tianjin 300161, China.

Guang-Dong Wang
Military Transportation Research Institute, Tianjin 300161, China.

Journal of Marine Science and Technology, Vol. 27, No. 6, pp. 481-497 (2019)
DOI: 10.6119/JMST.201912_27(6).0001

DYNAMIC RESPONSE ANALYSIS OF THE LIFTING LOAD SYSTEM OF A CRANE SHIP IN IRREGULAR WAVES

Xiao-Rong Yang [1,2], Qiu-Ming Gan[3] , Yan-Hong Wang[1] and Guang-Dong Wang [3]

Key words: a crane ship, the lifting load system, the coupling motion, irregular waves, nonlinear dynamic responses.

ABSTRACT

In this paper, the indirect time domain method is adopted to analyze the dynamic responses of a mooring crane ship. The motion equations of its lifting load system are derived from Lagrange's equations and the features of the coupling motion between the crane ship and its lifting load system are presented. The hydrodynamic coefficients of the crane ship are calculated on the base of 3D potential flow theory. The lumped-mass model is used to analyze the dynamic features of its mooring lines. The nonlinear features of the motion equations being taken into account, the displacements of the crane ship and the lifted cargo are calculated by using the time domain analysis. In particular, the angular displacements of the lifted cargo are calculated and the traces of the lifted cargo in space are represented when it is lifted or lowered at the speed of 0.6m/s. The response spectrums of the lifted cargo in sea state II are obtained by using the frequency domain analysis in irregular waves. They show that the range of angular displacement frequency in resonance state is wider than that in non-resonance state. In resonance state, the energy of the lifting load system is more concentrated and the peak values of the response spectrums of the lifted cargo are more obvious. The curves of the response spectrums present obvious nonlinear features. The analysis methods and calculated results of this paper are of reference value for offshore lifting engineers and designers.

I. INTRODUCTION

1. Research achievements of the lifting load system of a crane ship

Crane ships, also known as floating cranes, are widely used in harbor handling, bridge construction, ocean salvage and other ocean engineering work.

The wave factors must be taken into account when a crane ship is lifting cargoes at sea. On one hand, the lifted cargo will swing because of the motion of the crane ship, which can affect the accuracy of the lifting. On the other hand, the inertial force caused by the swing of the lifted cargo will act on the crane ship. As a result, the load on the ship will be increased. Therefore, the research of a crane ship is focused on predicting their responses to sea waves and the interaction between a crane ship and its lifted cargo.

Since 1970s, the development of the numerical method in ship motion research has promoted the study on the swing of the lifted cargo. Schellin et al. (1991) established the coupled motion equations between the crane ship and the lifted cargo, and discussed their coupled motion in regular waves. Schellin et al. (1991) investigated the motion response of a shear-leg crane ship which is lifting a heavy load in wave groups. The 9-DOF dynamic model incorporated hull motions which were coupled with nonlinear large-angle load swing and an elastic stretch of the hoisting rope. Clauss et al. (1992) analyzed the motion characteristics of a large crane barge, ship and SSCV (Semi-Submersible Crane Vessel) and found out that the motion behaviour of SSCVs is very complex, and depends on coupling of load swing and vessel motions. So heave, pitch, and roll resonance oscillations are mutually interfering with vertical and horizontal load motions. Kral et al. (1995) believed that qualitative changes in the dynamic behavior of offshore systems during operation are mainly caused by varying loads, which are caused by fluid-structure interactions and adopting nonlinear models. Balachandran (1999) investigated the planar control and proposed *mechanical filter concept*. It was shown that the presence of the filter helps in eliminating some of the subcritical bifurcations that may arise in the crane-load response during periodic ship-roll excitations. The presence of feedback control can also effectively suppress transient crane-load oscillations.

Henry et al. (2001) established the model of the lifting load system of a crane ship by using a rigid massless cable and massive point load. The results of the computer simulation

Paper submitted 04/27/18; revised 11/09/18; accepted 09/17/19. Author for correspondence: Xiao-Rong Yang (E-mail: Luai-yxr@163.com).
[1]Military Transportation University, Tianjin 300161, China.
[2] Tianjin University Renai College, Tianjin 301636, China.
[3] Military Transportation Research Institute, Tianjin 300161, China.

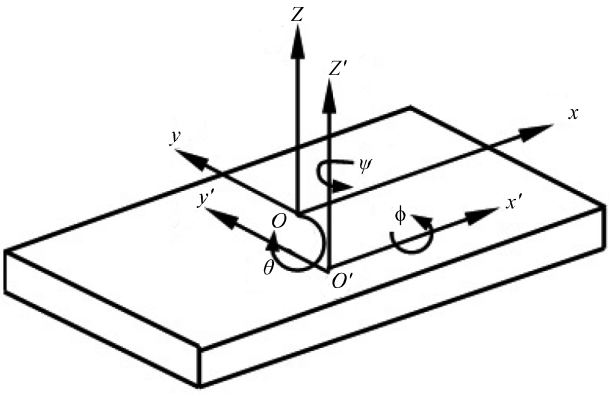

Fig. 1. Coordinate systems.

were verified by an experiment on a three-degree-of-freedom motion simulation platform of a ship. Chin et al.(2001) analyzed the dynamic response of a cable-suspended load and obtained the control method with multiple scales. Ellermann et al. (2002) conducted experimental and theoretical studies on the nonlinear dynamic responses of a moored crane vessel in regular waves. Many results of computations for two crane vessels, barge and ship were presented. Special attention was paid to oscillations near the frequencies of primary resonances and to subharmonic motions. An excellent agreement was found between the results of time-domain and frequency-domain analysis. With damping and response lag involved, Masoud et al. (2004) carried out the research on the response of lifting load system of a crane ship. The results demonstrated that the pendulations can be significantly reduced, and therefore the range of sea conditions in which cargo-transfer operations can take place can be greatly expanded. Cha et al. (2010) established the six-degree-of-freedom motion equation of the lifting load system, and the nonlinear terms in the equations of motion were considered. Sweiti et al. (2007) studied the cargo pendulation control of an elastic ship-mounted crane by using Maryland Rigging system. Simulation and experimental results showed that the expressed control strategy performs well and has a significant effect in controlling the vibrations of the crane for different operating conditions and payload masses. By using finite element method, Ren et al. (2008) established the models of a crane ship and its lifted cargo which is as a planar pendulum of point mass, and studied their dynamic responses. The calculation results showed that the large-amplitude responses occur at wave periods near the natural period of the payload. Load swing angle is smaller for crane-ship with flexible boom, in comparison with rigid boom. The ship surge motions have large vibrations for crane-ship with flexible boom, which were not observed for a rigid boom.

Wang et al. (2010) used an eight-degree-of-freedom model of time domain to simulate a moored crane ship motion numerically. The model included large-amplitude load swing, hydrodynamic memory effects, nonlinear drag forces, wave forces, and nonlinear restoring forces of a mooring system. Chen et al. (2011) discussed the motion responses of a large crane ship during lifting work and the effects of damping coefficient on them. The radius of inertia of a crane ship is calculated by using fluid dynamics and compared with that of a conventional vessel. The analysis result shows that a large crane ship working at sea is safe and reliable. Hu et al. (2012) constructed a double-degree-of-freedom pendulum model for a lifting load system based on the geometric constraints. The dynamic response of the lifting load system of a 3000 tons crane was calculated in regular waves. Hong et al. (2012) developed a dynamic model of a container crane mounted on a ship, which included both sea-wave-induced ship motion and ship-motion-induced container sway. Heading sea (following sea), quartering sea and beam sea conditions were considered in simulation. Simulation results reveal that the waves coming from 900 will make more effects on the sway angles and it should be avoided in operating mobile harbor. Ngo et al. (2012) designed a sliding surface in which the longitudinal sway of the load is incorporated with the trolley dynamics. The asymptotic stability of the closed-loop system is guaranteed by a control law derived for the purpose. The proposed new mechanism can suppress lateral sway, which functionality is not possible with conventional cranes

2. Contents of this paper

The above mentioned research achievements show that the coupling, nonlinear and random motions caused by irregular waves are the features of the lifting load system of a crane ship, but in the analysis of the motion of the lifting load system, the above mentioned literatures has only taken some of the factors into consideration. The conclusions do not correspond with the actual situation very well.

In this paper, we not only take the coupling, nonlinear and random motions into account, but also analyze the dynamic responses of the lifting load system in irregular waves. In particular, the angular displacements of the lifted cargo are calculated and its traces in space are described when it is lifted or lowered at the speed of 0.6m/s.

Assuming that the swing of the lifted load has little impact on the motion responses of the crane ship, the one-way coupled analysis between a crane ship and its lifting load system is performed in this paper. A three-degree-of-freedom model is adopted to study the motion of the lifting load system because Cha et al. (2010) has proved that the increase in the degree of freedom has little impact on the motion of the lifting load system. In addition, considering the fact that a mooring system has great impacts on the horizontal direction motion of a crane ship, we do not use coefficients of restitution as the equivalents of mooring restoring forces as is described by Masoud et al. (2004). Instead, we make dynamic analysis of the mooring system to obtain more accurate solution. We adopt random irregular wave theory to calculate the responses of the crane ship and its lifting load system.

II. MOTIONS OF A CRANE SHIP

A working crane ship can be regarded as a moored floating body with no speed. Considering the nonlinear features of mooring recovery forces, wind-forces and wave-forces, we adopt a time domain model to achieve the motion responses of a crane ship.

1. Coordinate systems

As is shown in Fig.1, two right-handed coordinate systems are defined:

1 *O-xyz* fixed in space, with *O* in the still water surface, *x* in the direction of the wave propagation and *z* in the upward direction.

2 *O'-x'y'z'* moving with the ship' speed, with *O'* above or below the average position of the ship's center of gravity, *x'* parallel to still water surface, *y'* also parallel to still water surface and *z'* in the upward direction. The angular motions of the body about axes are denoted by: ϕ,θ,ψ

2. Equations of motion of a crane ship

The equations of motion of a crane ship are expressed as Eq. (1) with Cummins equation (Cummins, 1962).

$$\mathbf{M}\ddot{\mathbf{X}}(t)+\mathbf{A}(\infty)\ddot{\mathbf{X}}(t)+\int_0^t \mathbf{K}(t-\tau)\dot{\mathbf{X}}(\tau)d\tau+\mathbf{C}\mathbf{X}(t)=\mathbf{F}(t) \tag{1}$$

where $\mathbf{X}(t)$ is the translational or rotational displacement vector in direction of the crane ship, $\dot{\mathbf{X}}(t)$ is the translational or rotational velocity vector in direction of the crane ship, $\ddot{\mathbf{X}}(t)$ is the translational or rotational acceleration vector in direction of the crane ship, $\mathbf{M}$ is the mass matrix of the crane ship, $\mathbf{A}(\infty)$ is the constant additional mass matrix, $\mathbf{K}(t)$ is the retardation function matrix, $\mathbf{C}$ is the restoring spring coefficient matrix of static water and $\mathbf{F}(t)$ are external loads acting on the crane ship, which can be expressed as Eq. (2):

$$\mathbf{F}(t)=\mathbf{F}_{\mathbf{w1}}(t)+\mathbf{F}_{\mathbf{w2}}(t)+\mathbf{F}_{\mathbf{cu}}(t)+\mathbf{F}_{\mathbf{wi}}(t)+\mathbf{F}_{\mathbf{v}}(t)+\mathbf{F}_{\mathbf{m}}(t) \tag{2}$$

where $\mathbf{F}_{\mathbf{w1}}(t)$ and $\mathbf{F}_{\mathbf{w2}}(t)$ are respectively the first order and the second order wave force vectors, $\mathbf{F}_{\mathbf{cu}}(t)$ is the current force vector, $\mathbf{F}_{\mathbf{wi}}(t)$ is the wind force vector, $\mathbf{F}_{\mathbf{v}}(t)$ is the viscous damping force vector and $\mathbf{F}_{\mathbf{m}}(t)$ is the mooring force vector.

3. Wave forces and hydrodynamic coefficients

(1) Wave force transfer function and hydrodynamic coefficients in frequency domain

On the basis of 3D potential flow theory, the source-sink distribution method is used to obtain wave force transfer function $H(\omega)$ (shown in Eq. (3)) and hydrodynamic coefficients in frequency domain, which include the additional mass matrix $\mathbf{A}(\omega)$ and the potential flow damping matrix $\mathbf{B}(\omega)$. The j[th] component of $\mathbf{A}(\omega)$ and $\mathbf{B}(\omega)$ matrixes is expressed respectively in Eqs. (4) and (5) (Dai, 2008).

$$H_k(\omega)=i\rho\omega\iint_S \phi_0\vec{n}_k ds \tag{3}$$

$$a_{kj}(\omega)=\rho\iint_S \mathrm{Re}(\varphi_j)\vec{n}_k ds \tag{4}$$

$$b_{kj}(\omega)=\rho\iint_S \mathrm{Im}(\varphi_j)\vec{n}_k ds \tag{5}$$

where S is the wetted surface of the crane ship, ρ is water density, ϕ_0 is the velocity potential of incident waves with unit amplitudes, φ_j is the velocity potential of radiation waves caused by a displacement in direction j when the crane ship makes the unit amplitude motion with frequency ω. The velocity potential of radiation wave φ_j is calculated with Green function that is expressed as Eq. (6):

$$\phi_j(p)=\frac{1}{4\pi}\iint_S\left\{G(p,q)\frac{\partial}{\partial n_q}\left[\phi_j(q)\right]-\phi_j(q)\frac{\partial}{\partial n_q}\left[G(p,q)\right]\right\}ds_q \tag{6}$$

where p is these dots in the flow field, q is these dots on the surface of the crane ship.

(2) Wave forces and the retardation function in time domain (Xiao, 2006)

$$h_k(t)=\frac{1}{\pi}\int_0^\infty\left\{\mathrm{Re}\left[H_k(\omega)\right]\cos\omega t-\mathrm{Im}\left[H_k(\omega)\right]\sin\omega t\right\}d\omega \tag{7}$$

$$F_{wk}(t)=\int_0^t h_k(\tau)\varepsilon(t-\tau)dt \tag{8}$$

Eq. (7) is the time domain expression of one order wave pulse function while Eq. (8) is that of one order wave force. Eq. (9) is the retardation function while Eq. (10) is the constant additional mass.

$$k_{ij}(t)=\frac{2}{\pi}\int_0^\infty b_{ij}(\omega)\cos\omega t dt \tag{9}$$

where $b_{ij}(\omega)$ is the potential flow damping (shown in Eq. (5)) .

$$a_{ij}(\infty)=a_{ij}(\omega)+\frac{1}{\omega}\int_0^\infty k_{ij}(t)\sin\omega t dt \tag{10}$$

where $a_{ij}(\omega)$ is the additional mass (shown in Eq. (4)).

4. Viscous damping forces

When a crane ship is in motion, the friction between the ship and water and the viscous effect of water produce the viscous damping forces, which are proportional to the second-order of the ship speed. Empirically, the viscous damping forces of the three degrees of freedom in horizontal plane can be expressed as

(Journee, 1993):

$$\begin{cases} F_{v1} = -\dfrac{1}{2}\rho C_D BD|\dot{x}|\dot{x} \\ F_{v2} = -\dfrac{1}{2}\rho C_D LD|\dot{y}|\dot{y} \\ F_{v6} = -\dfrac{1}{6}\rho C_D L^3 D|\dot{\psi}|\dot{\psi} \\ C_D = 1.50 \end{cases} \tag{11}$$

where F_{V1}, F_{V2}, F_{V6} are respectively nonlinear viscous surge damping, nonlinear viscous sway damping, nonlinear viscous yaw damping, ρ is water density, L、B、D are respectively the length, the width and the draught of the crane ship, $\dot{x}, \dot{y}$ are the velocities at which the crane ship moves respectively in directions *x* and *y* and $\dot{\psi}$ is the angular velocity at which the coordinate system O'-x'y'z ' rotates around z axis(shown in Fig. 1).

5. Mooring restoring forces

The forces acting on the micro-segment of a mooring line are shown in Fig. 2, where R_x, R_y, R_z are unit drag forces, e_x, e_y, e_z are additional masses and a_x, a_y, a_z are accelerations in *x*, *y* and *z* directions respectively, T is the tension, ds is the length, EA is the axial stiffness, γ is the included angle between the micro-segment and *xoy*-plane, α is the included angle between the projection of the micro-segment in *xoy*-plane and *oy* axis and W is the weight of unit length.

(1) Static differential equations

The static differential equations of the micro-segment of a mooring line can be obtained on the basis of relationships shown in Fig. 2.

$$\begin{cases} \dfrac{dT}{ds} = W\sin\gamma - (1+\dfrac{T}{EA})\cdot\dfrac{1}{2}\rho c_{dt} D_m |v_t| v_t \\ T\dfrac{d\gamma}{ds} = W\cos\gamma + (1+\dfrac{T}{EA})\cdot\dfrac{1}{2}\rho c_{dn} D_m |v_n| v_n \\ dx = ds\cdot\cos\gamma\sin\alpha \\ dy = ds\cdot\cos\gamma\cos\alpha \\ dz = ds\cdot\sin\gamma \end{cases} \tag{12}$$

where ρ is water density, D_m is the diameter of the cross-section, c_{dt} and c_{dn} are the drag force coefficients, v_t and v_n are respectively the water flow velocities on the tangent and the normal of the micro-segment. By using the boundary conditions, the pre-tension of a mooring line or the displacements of its ends, we obtain the static configuration of the mooring line and make its dynamic analysis.

(2) Equations of motion

The equation of motion of the i^{th} micro-segment of a mooring line is shown as follows:

$$(M_i + A_i)\ddot{\mathbf{X}}_i(t) = \mathbf{F}_i(t) \tag{13}$$

where $\mathbf{F}_i(t)$ is the force vector acting on the i^{th} micro-segment, $\ddot{\mathbf{X}}_i(t)$ is the acceleration vector of the i^{th} micro-segment of the mooring line, M_i and A_i are the mass and the additional mass respectively. Eq. (13) is transformed into a component form as follows (Tang, 2009):

where A_i is the additional mass, $\mathbf{f}_d$ represents the drag force vector and $B_i ds_i$ is the volume. Eq. (15) and Eq. (16) are the expressions of A_i and $\mathbf{f}_d$ respectively.

$$\begin{bmatrix} m_i & 0 & 0 \\ 0 & m_i & 0 \\ 0 & 0 & m_i \end{bmatrix}\begin{bmatrix} \ddot{x}_i \\ \ddot{y}_i \\ \ddot{z}_i \end{bmatrix} + A_i \begin{bmatrix} \cos^2\gamma\cos^2\alpha+\sin^2\gamma & -\cos^2\gamma\sin\alpha\cos\alpha & -\cos\gamma\sin\alpha\sin\gamma \\ -\cos^2\gamma\sin\alpha\cos\alpha & \cos^2\gamma\sin^2\alpha+\sin^2\gamma & -\cos\gamma\cos\alpha\sin\gamma \\ -\cos\gamma\sin\alpha\sin\gamma & -\cos\gamma\cos\alpha\sin\gamma & \cos^2\gamma \end{bmatrix}_i \begin{bmatrix} \ddot{x}_i \\ \ddot{y}_i \\ \ddot{z}_i \end{bmatrix}$$
$$= \begin{bmatrix} T\sin\alpha\cos\gamma \\ T\cos\alpha\cos\gamma \\ T\sin\gamma \end{bmatrix}_i - \begin{bmatrix} T\sin\alpha\cos\gamma \\ T\cos\alpha\cos\gamma \\ T\sin\gamma \end{bmatrix}_{i-1} + \begin{bmatrix} f_{dx_1} \\ f_{dx_2} \\ f_{dx_3} \end{bmatrix} - \begin{bmatrix} 0 \\ 0 \\ m_i g - \rho g B_i ds_i \end{bmatrix} \tag{14}$$

$$A_i = \frac{\pi D_m^2}{4}\rho c_a ds \tag{15}$$

where c_a is the additional mass coefficient.

$$\mathbf{f}_d = \frac{1}{2}\rho \mathbf{c}_d D_m ds |\mathbf{u}|\mathbf{u} \tag{16}$$

where $\mathbf{c}_d$ is the vector of the drag force coefficient, $\mathbf{u}$ is the velocity vector of the i^{th} micro-segment of the mooring line.

The other symbols are shown in Fig. 2.

Eq. (14) is solved to get the tension of the mooring line with Houbolt differential format expressed as follows (Zhang, 2007):

$$\ddot{s}_i^{n+1} = (2s_i^{n+1} - 5s_i^n + 4s_i^{n-1} - s_i^{n-2})/\Delta t^2 \tag{17}$$

$$\ddot{s}_i^{n+1} = (11s_i^{n+1} - 18s_i^n + 9s_i^{n-1} - 2s_i^{n-2})/6\Delta t \tag{18}$$

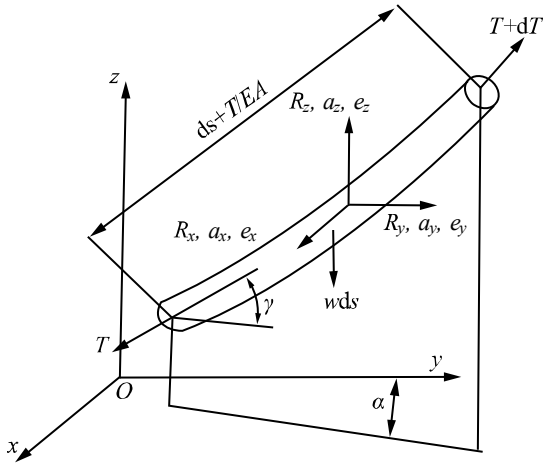

Fig. 2. Forces acting on the micro-segment of a mooring line.

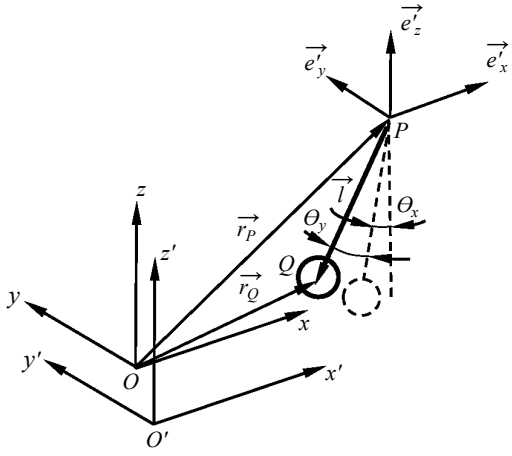

Fig. 3. Coordinates of the lifting load system.

III. MOTION EQUATIONS OF THE LIFTING LOAD SYSTEM

The experimental and analytical results made by Todd et al. (1997) show that the lifted cargo of a crane ship has the dynamic features of spherical pendulum under forced vibration, so its motion in space is described with three degrees of freedom: in-plane angle, out-plane angle and the sling length.

The lifting load system of a crane ship includes the hanging point (represented by P in Fig. 3), the sling and the lifted cargo (represented by Q in Fig. 3). The weight of the sling is not considered.

1. Coordinates of the lifting load system

In Fig. 3, $\vec{r}_P$ and $\vec{r}_Q$ are respectively the space position vectors of the hanging point P and the lifted cargo Q in coordinate system *o-xyz*. $\vec{l}$ is the sling length vector. θ_x is the in-plane angle, the included angle between the projection of the sling on *x'o'z'*-plane and *o'z'* axis. θ_y is the out-plane angle, the included angle between the sling and *x'o'z'*-plane. $\vec{l}$ 、θ_x and θ_y are defined to analyze the motion of the lifted cargo in coordinate system *O'-x'y'z* $\vec{e}_{x'}$ 、$\vec{e}_{y'}$ and $\vec{e}_{z'}$ are unit vectors of coordinate system *O'-x'y'z*, which are respectively parallel to x', y' and z' axis.

2. Relationship between displacements of the lifting load system

In coordinate system *O-xyz*, the coordinates of any point (represented by *A)* of the crane ship are expressed as (Michael Harnett., 2000):

$$\begin{bmatrix} x_A & y_A & z_A \end{bmatrix}^T = \begin{bmatrix} x_G & y_G & z_G \end{bmatrix}^T + \mathbf{T_o} \cdot \begin{bmatrix} x'_A & y'_A & z'_A \end{bmatrix}^T \quad (19)$$

where $\begin{bmatrix} x'_A & y'_A & z'_A \end{bmatrix}$ are the coordinates of the point A in coordinate system *O'-x'y'z'*, $\begin{bmatrix} x_G & y_G & z_G \end{bmatrix}$ are the coordinates of the gravity center of the crane ship in coordinate system *o-xyz*, and $\mathbf{T_O}$ is the coordinate transform matrix which is expressed as follows:

$$\mathbf{T_o} = \begin{bmatrix} 1 & -\psi & \theta \\ \psi & 1 & -\phi \\ -\theta & \phi & 1 \end{bmatrix} \quad (20)$$

where ϕ, θ, ψ are the rotating angles of the coordinate system *O'-x' y' z* ' around *x*, *y*, *z* axis (shown in Fig. 1).

If the coordinates of the hanging point P are $(x_{p'}, y_{p'}, z_{p'})$ in the coordinate system *O'-x' y' z* ', on the basis of Eq. (19), its coordinates, speeds and accelerations in the coordinates system *O-xyz* are expressed as follows:

$$\begin{cases} [x_p \, y_p \, z_p]^T = [x_G \, y_G \, z_G]^T + \mathbf{T_o}[x_{p'} \, y_{p'} \, z_{p'}] \\ [\dot{x}_p \, \dot{y}_p \, \dot{z}_p]^T = [\dot{x}_G \, \dot{y}_G \, \dot{z}_G]^T + \dot{\mathbf{T}}_\mathbf{o}[x_{p'} \, y_{p'} \, z_{p'}] \\ [\ddot{x}_p \, \ddot{y}_p \, \ddot{z}_p]^T = [\ddot{x}_G \, \ddot{y}_G \, \ddot{z}_G]^T + \ddot{\mathbf{T}}_\mathbf{o}[x_{p'} \, y_{p'} \, z_{p'}] \end{cases} \quad (21)$$

In Eq. (21), $\mathbf{T_O}$ is the coordinate transform matrix.

In Fig. 3,

$$\vec{r}_Q = \vec{r}_P + \vec{l} \quad (22)$$

On the base of Eq. (22), the coordinates of the lifted cargo Q in the coordinate system *O-xyz* are derived:

$$\begin{cases} x_q = x_p - l \sin\theta_x \cos\theta_y \\ y_q = y_p + l \sin\theta_y \\ z_q = z_p - l \cos\theta_x \cos\theta_y \end{cases} \quad (23)$$

Table 1. Main parameters of the sample crane ship.

Content	Symbol	Value	Unit
Ship length	L	110	m
Ship width	B	46	m
Ship Draft	D	2.75	m
Block coefficient	C_b	0.952	—
Tonnage	△	13582.1	ton
Distances of gravity center to baseline	x_g	0	m
	y_g	0	
	z_g	4	
Turning radius	k_{xx}	13.9	m
	k_{yy}	32.3	
	k_{zz}	35.1	
Coordinates of point P (related to gravity center)	x_p	120	m
	y_p	0	
	z_p	116	
Lifting capacity	M	1300	ton

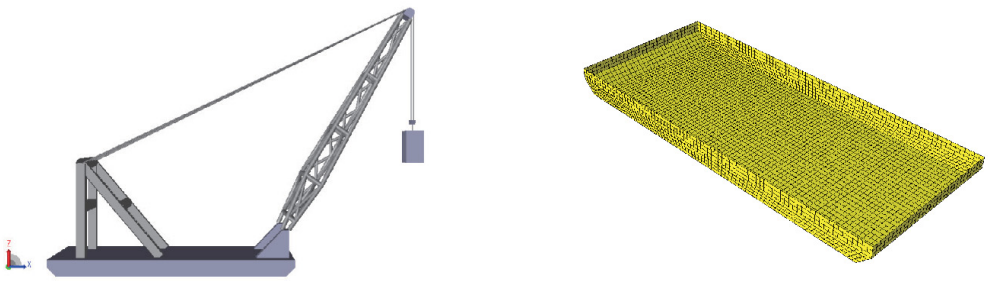

Fig. 4. The model of the sample crane ship and its wet surface grid.

where $[x_p, y_p, z_p]$ are the coordinates of the hanging point P in the coordinate system *O-xyz*.

3. Motion equations of the lifting load system

The following is Lagrange equation which can be used to derive the equations of motion of the lifting load system (Li, 2002):

$$\frac{d}{dt}\left(\frac{\partial T}{\partial \dot{q}_i}\right)-\frac{\partial T}{\partial q_i}+\frac{\partial V}{\partial q_i}=Q_i \tag{24}$$

The kinetic energy of the lifting load system is:

$$T=\frac{1}{2}m\dot{x}_q^2(t)+\frac{1}{2}m\dot{y}_q^2(t)+\frac{1}{2}m\dot{z}_q^2(t) \tag{25}$$

where m is the mass of the lifted cargo and $[x_q, y_q, z_q]$ from Eq. (23) are the coordinates of the lifted cargo Q in the coordinate system *O-xyz*.

When the *xoy* plane is regarded as zero potential energy plane, on the base of Eq. (23), the potential energy of the lifting load system is expressed by Eq. (26):

$$V=mgz_q(t)=mg[z_p(t)-l(t)\cos\theta_x(t)\cos\theta_y(t)] \tag{26}$$

where g is the gravity acceleration.

Substituting Eq. (25), Eq. (26) for the T and V in the Eq. (24), setting $q_1=x_p$, $q_2=y_p$, $q_3=z_p$ in Eq. (24) and adopting the relationship expressed in Eq. (23), we obtain the second-order differential equations of the in-plane θ_x, out-plane angle θ_y and the sling length $l(t)$, which are expressed by Eq. (27):

$$\begin{cases}\left[\ddot{\theta}_x(t)+2n\dot{\theta}_x(t)\right]\cos\theta_y(t)+2\frac{\dot{l}(t)}{l(t)}\dot{\theta}_x(t)\cos\theta_y(t)-2\dot{\theta}_x(t)\dot{\theta}_y(t)\sin\theta_y(t)-\\ \frac{1}{l(t)}\cos\theta_x(t)\left[\ddot{x}_p(t)+2n\dot{x}_p(t)\right]+\frac{1}{l(t)}\sin\theta_x(t)\left[\ddot{z}_p(t)+2n\dot{z}_p(t)\right]+\frac{g}{l(t)}\sin\theta_x(t)=0\\ \ddot{\theta}_y(t)+2\frac{\dot{l}(t)}{l(t)}\dot{\theta}_y(t)+\dot{\theta}_x^2(t)\sin\theta_y(t)\cos\theta_y(t)+\frac{1}{l(t)}\sin\theta_x(t)\sin\theta_y(t)\left[\ddot{x}_p(t)+2n\dot{x}_p(t)\right]+\\ \frac{1}{l(t)}\cos\theta_y(t)\left[\ddot{y}_p(t)+2n\dot{y}_p(t)\right]+\frac{1}{l(t)}\sin\theta_y(t)\cos\theta_x(t)\left[\ddot{z}_p(t)+2n\dot{z}_p(t)\right]+\frac{g}{l(t)}\sin\theta_y(t)\cos\theta_x(t)=0\end{cases} \tag{27}$$

where $[x_p, y_p, z_p]$ are the coordinates of the hanging point P in the coordinate system *O-xyz*.

In Eq. (27), the damping of the lifting load system is taken into account and a certain percentage of the critical damping is

Table 2. Parameters of the mooring line.

Length	Diameter	Underwater weights	Axial stiffness	Pre-tension	Pre-tension angle	Drag coefficient	Added mass coefficient
m	m	kg/m	MN	kN	deg	Cd	Ca
753.7	0.102	205.8	908.46	3.074e6	29.6	1.2	1.7

Table 3. Environmental conditions.

	Water depth	Significant wave height Hs	Zero-crossing period Tz
Sea state I	200m	0.1m	5.8s
Sea state II	200m	0.5m	7.0s
Sea state III	200m	1.0m	7.8s

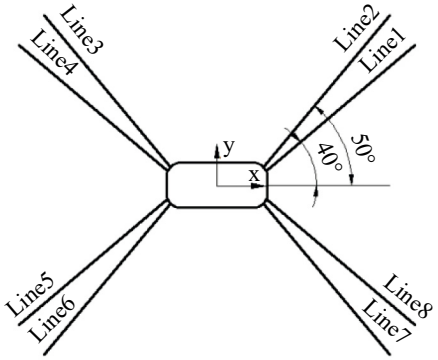

Fig. 5. Mooring system.

acted on the lifted cargo Q. n is the damping coefficient. The damping ratio ξ is usually selected from 0.5% to 1% in order to determine the damping coefficient n (Masoud et al. 2004). In this paper, the damping coefficient n is :

$$n = \xi\sqrt{\frac{g}{l}} \tag{28}$$

where g is the gravity acceleration and l is the sling length.

IV. SAMPLE CRANE SHIP AND ITS PARAMETERS

The model of the sample crane ship and its wet surface grid are shown in Fig. 4.

1. Main parameters of the sample crane ship

The main parameters of the sample crane ship are shown in Table 1.

2. Parameters of the mooring system of the sample crane ship

A scattered mooring system is adopted to locate the working crane ship. This system is divided into four groups and each group has two mooring lines, the arrangement of which is shown in Fig. 5.

The parameters of the mooring lines are shown in Table 2.

3. Wave spectrum and environmental conditions

How sea waves are caused by wind is a complicated process, so it is difficult to obtain a theoretical estimation of their spectrum by using the parameters of the wind. Currently, sea wave spectrums are derived from a great quantity of datum acquired from experience as well as by theoretical analysis. In this paper, Pierson-Moskowitz spectrum is adopted as sea wave spectrum which is expressed in Eq. (29). (Wu, 1988).

$$S(\omega) = \frac{a}{\omega^5}\exp\left(\frac{b}{\omega^4}\right) \tag{29}$$

where:

$$b = \left(\frac{2\pi}{T_z}\right)^4 \tag{30}$$

$$a = \frac{bH_s^2}{4} \tag{31}$$

The surface elevation of irregular wave, when expressed by Pierson-Moskowitz spectrum, is:

$$\zeta(t) = \sum_{1}^{N}\sqrt{2S(\omega_j)\Delta\omega}\cdot\sin(\omega_j t + \varepsilon_j) \tag{32}$$

Sea states I, II and III are chosen as the environmental conditions in calculating motion responses of the lifting load system. The parameters of these sea states are shown in Table 3. The P-M spectrums in the sea states in Table 3 are shown in Fig. 6. In sea state I, the significant wave height is 0.1m which represent a calm sea. In sea state II, the significant wave height is 0.5m which represent the main working condition of the crane ship. In sea state III, the significant wave height is 1.0m which represent the strong sea state where the crane ship is considered to stop working.

Table 4. Calculation parameters.

	Wave direction deg	Wave frequency rad/s	Wave height m	Sling length m	Lifting (lowering)velocity m/s
Working condition I	0	0.82	1.2	50	0
Working condition II	30	0.82	1.2	50	0
Working condition III	90	0.82	1.2	50	0

Table 5. Maximum displacements of the lifted cargo with different wave directions.

Wave direction（deg）	0	30	90
In-plane angle（deg）	0.89	1.25	0.41
Out-plane angle（deg）	0	0.82	2.91

Table 6. Calculation parameters.

	Wave direction Deg	Wave frequency rad/s	Wave height m	Sling length m	Lifting (lowering)velocity m/s
Working condition I	30	0.82	1.2	50	0
Working condition II	30	0.82	0.6	50	0

Table 7. Maximum displacements of the lifted cargo with different wave heights.

Wave height（m）	0.6	1.2
In-plane angle（deg）	0.32	1.25
Out-plane angle（deg）	0.43	0.82

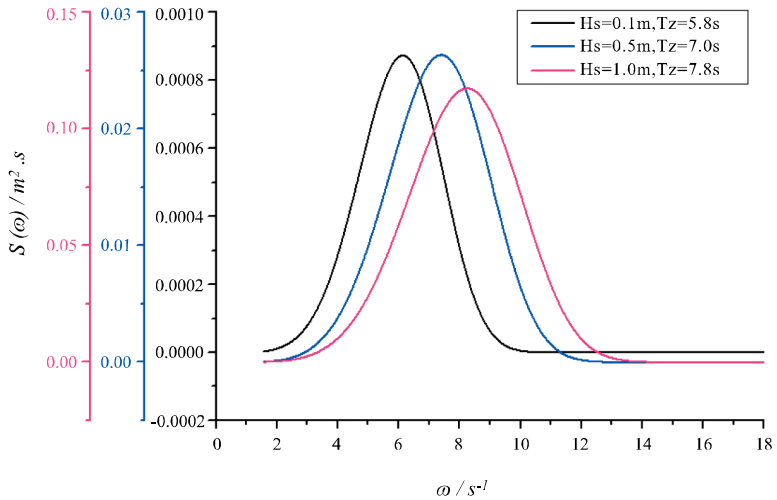

Fig. 6. Pierson-Moskowitz spectrum.

V. RESULTS AND DISCUSSION

1. Displacements of the lifted cargo in regular waves

In this paper, we calculate the displacements of the lifted cargo in regular waves firstly.

(1) The displacements of the lifted cargo with different wave directions.

The calculation parameters and the maximum motion amplitudes of the crane ship are shown respectively in Table 4 and Table 5.

(2) The displacements of the lifted cargo with different wave heights.

Table 8. Calculation parameters.

	Wave direction	Wave frequency	Wave height	Sling length	Lifting (lowering)velocity
	deg	rad/s	m	m	m/s
Working condition I	30	0.82	1.2	50	0
Working condition II	30	0.53	1.2	50	0
Working condition III	30	0.71	1.2	50	0
Working condition IV	30	0.90	1.2	50	0

Table 9. Maximum displacements of the lifted cargo with different wave frequencies.

Wave frequency（rad/s）	0.53	0.71	0.82	0.90
In-plane angle（deg）	1.99	0.99	1.25	0.57
Out-plane angle（deg）	1.14	0.68	0.82	0.56

Table 10. Calculation parameters.

	Wave direction	Wave frequency	Wave height	Sling length	Lifting (lowering)velocity
	deg	rad/s	m	m	m/s
Working condition I	30	0.53	1.2	70.0	0
Working condition II	30	0.53	1.2	50.0	0
Working condition III	30	0.53	1.2	34.9	0
Working condition IV	30	0.53	1.2	20.0	0

Table 11. Maximum displacements of the lifted cargo with different sling lengths.

Sling length（m）	20	34.9	50	70
In-plane angle（deg）	3.01	18.78	1.99	0.68
Out-plane angle（deg）	1.50	22.36	1.14	0.55

Table 12. Calculation parameters.

	Wave direction	Wave frequency	Wave height	Sling initial length	Lifting (lowering)velocity
	deg	rad/s	m	m	m/s
Working condition I	30	0.53	1.2	60	0.05
Working condition II	30	0.53	1.2	60	0.10
Working condition III	30	0.53	1.2	10	-0.05
Working condition IV	30	0.53	1.2	10	-0.10

The calculation parameters and the maximum motion amplitudes of the crane ship are shown respectively in Table 6 and Table 7.

(3) The displacements of the lifted cargo with different wave frequencies.

The calculation parameters and the maximum motion amplitudes of the crane ship are shown respectively in Table 8 and Table 9.

(4) The displacements of the lifted cargo with different sling lengths.

The calculation parameters and the maximum motion amplitudes of the crane ship are shown respectively in Table 10 and Table 11.

(5) The displacements of the lifted cargo with lifting (lowering) velocities.

The calculation parameters and the maximum motion amplitudes of the crane ship are shown respectively in Table 12 and Table 13.

2. Displacements and trace of the lifted cargo in irregular waves

The waves involved in this paper are long-crested irregular waves composed of a series of superimposed linear waves.

Table 13. Maximum displacements of the lifted cargo in lifting and lowering.

	Lifting velocity 0.1m/s	Lifting velocity 0.05m/s	Lowering velocity -0.1m/s	Lowering velocity -0.05m/s
In-plane angle（deg）	15.08	18.23	11.13	15.19
Out-plane angle（deg）	15.90	13.19	4.78	8.34

Table 14. Maximum motion amplitudes of the crane ship.

	Hs=0.1m	Tz=5.8s	Hs=0.5m	Tz=7.0s	Hs=1.0m	Tz=7.8s
Wave directionsβ	0°	30°	0°	30°	0°	30°
Surge(m)	0.005	0.004	0.037	0.033	0.082	0.077
Sway(m)	8.85e-9	0.004	7.55e-8	0.025	1.25e-6	0.066
Heave(m)	0.017	0.016	0.122	0.119	0.265	0.257
Roll(deg)	2.25e-8	0.018	3.61e-7	0.129	9.72e-6	0.374
Pith(deg)	0.016	0.014	0.114	0.097	0.245	0.205
Yaw(deg)	9.28e-9	0.007	7.96e-8	0.008	3.38e-6	0.103

Table 15. Maximum displacements of the lifted cargo.

	In-plane angle（deg）		Out-plane angle（deg）		Displacement x（m）		Displacement y（m）		Displacement z（m）		Sling length（m）
Wave directions β	0°	30°	0°	30°	0°	30°	0°	30°	0°	30°	
Sea state I	0.05	0.04	5.6e-8	0.05	0.01	0.01	1.8e-8	0.01	0.05	0.04	50
	1.49	1.77	2.7e-6	1.7°	0.23	0.26	4.1e-7	0.27	0.05	0.05	8.35
Sea state II	0.33	0.26	3.8e-7	0.31	0.11	0.10	1.7e-7	0.09	0.35	0.32	50
	14.92	12.11	1.1e-5	10.19	3.20	2.60	2.6e-6	2.25	0.57	0.42	12.16
Sea state III	0.92	0.78	8.5e-7	0.60	0.42	0.38	5.1e-7	0.21	0.75	0.68	50
	29.24	29.59	3.2e-5	31.83	7.56	7.53	8.6e-6	7.96	2.30	2.71	15.10

Table 16. Calculation parameters.

	Wave directions β	Initial sling length	Velocity	
Sea state I	0°, 30°	65m	Lifting	0.06m/s
		6m	Lowering	-0.06m/s
Sea state II	0°, 30°	65m	Lifting	0.06m/s
		6m	Lowering	-0.06m/s
Sea state III	0°, 30°	65m	Lifting	0.06m/s
		6m	Lowering	-0.06m/s

Table 17. Maximum displacements of the lifted cargo in lifting and lowering.

		In-plane angle（deg）		Out-plane angle（deg）		Displacement x（m）		Displacement y（m）	
Wave directions β		0°	30°	0°	30°	0°	30°	0°	30°
Sea state I	Lifting	0.82	0.91	4.3e-6	1.34	0.15	0.13	5.5e-7	0.18
	Lowering	0.80	0.92	1.2e-6	1.19	0.17	0.19	3.5e-7	0.25
Sea state II	Lifting	8.79	8.04	3.2e-5	7.54	1.99	1.52	4.0e-6	1.59
	Lowering	4.27	4.40	8.7e-6	5.85	1.08	1.19	3.5e-6	1.21
Sea state III	Lifting	8.04	6.32	1.4e-5	6.15	2.32	1.79	2.7e-6	1.39
	Lowering	8.18	8.54	2.0e-5	10.23	2.93	2.67	8.1e-6	2.14

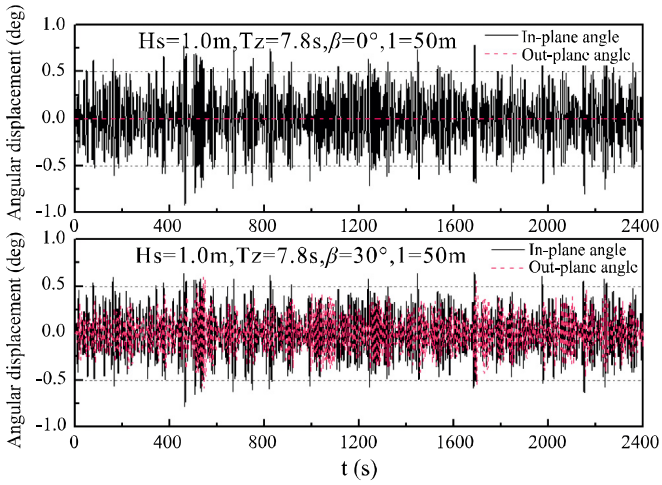

Fig. 7. Angular displacements of the lifted cargo.

$Hs = 0.1m, Tz = 5.8s, l = 50m$

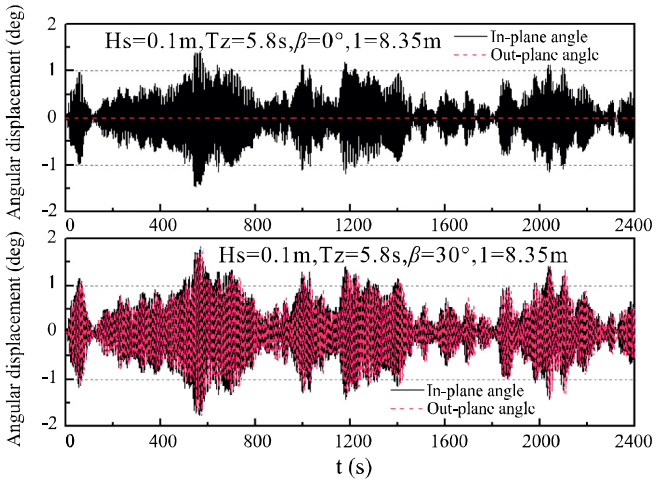

Fig. 8. Angular displacements of the lifted cargo.

$Hs = 0.1m, Tz = 5.8s, l = 8.35m$

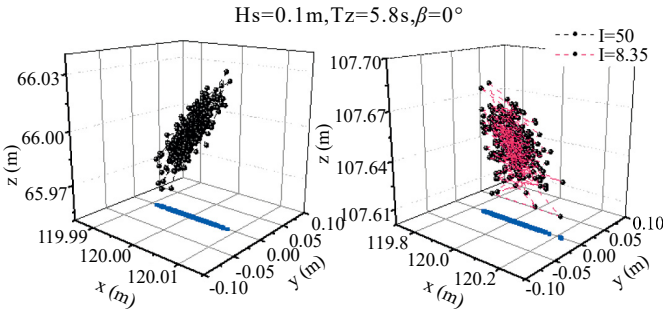

Fig. 9. Trace of the lifted cargo in space.

$Hs = 0.1m, Tz = 5.8s, \beta = 0°$

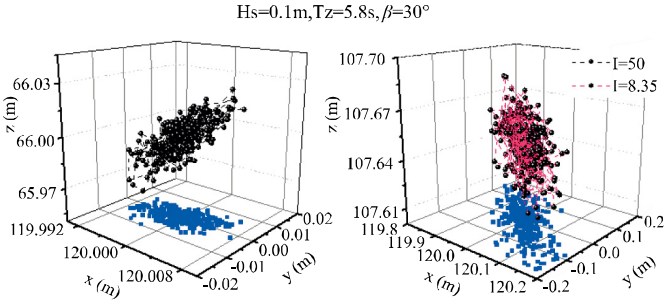

Fig. 10. Trace of the lifted cargo in space.

$Hs = 0.1m, Tz = 5.8s, \beta = 30°$

The wave directions are the head sea waves (β=0°) and the first oblique waves (β=30°). The parameters of their spectrum and the maximum motion amplitudes of the crane ship are shown respectively in Table 3 and Table 14.

(1) Displacements and trace of the lifted cargo with different sling lengths

The lifting load system of a crane ship includes the hanging point (represented by P in Fig. 3), the sling and the lifted cargo (represented by Q in Fig. 3). The natural frequency of the lifting load system varies with the length of sling. The natural frequencies of the lifting load system equal to the frequencies of external excitation and resonances occur in the system when the lengths of sling are respectively 8.35, 12.16, and 15.1 m. The displacements of the lifted cargo are the largest when resonances occur in the lifting load system.

Therefore, we choose 50m as the non-resonant length and the 8.35m, 12.16m and 15.1m as the resonant ones to calculate the displacements and trace of the lifted cargo in this paper, which are shown in Table 15 and in Fig.7-Fig.18.

A. Angular displacements and trace of the lifted cargo in sea state I.

B. Angular displacements and trace of the lifted cargo in sea state II.

C. Angular displacements and trace of the lifted cargo in sea state III.

From Fig. 7 to Fig. 18, we can find whether in regular or irregular waves, when working in the head sea, the motion of the crane ship is single degree of freedom, the in-plane and out-plane angle coupling effect is not obvious. However, in oblique waves, especially in irregular waves, the coupling effect is obvious, which shows nonlinear motion features of the lifted cargo. It is especially true in the resonant region where the maximum angular displacement of the lifted cargo is larger than that in head sea.

The resonance length of the sling increases with the increase of the wave period. In sea state I, the wave period is 5.8s while the resonance length is 8.35m, in sea state II, the wave period is 7.0s while the resonance length is12.16m, and in sea state III, the wave period is 7.8s while the resonance length is 15.1m.

As for the lifted cargo, its resonance displacement is much bigger than its non-resonance displacement. From Table 5, it can be found that in the case of head sea, its maximum horizontal resonance displacement is 0.23m at 0.1m wave height,

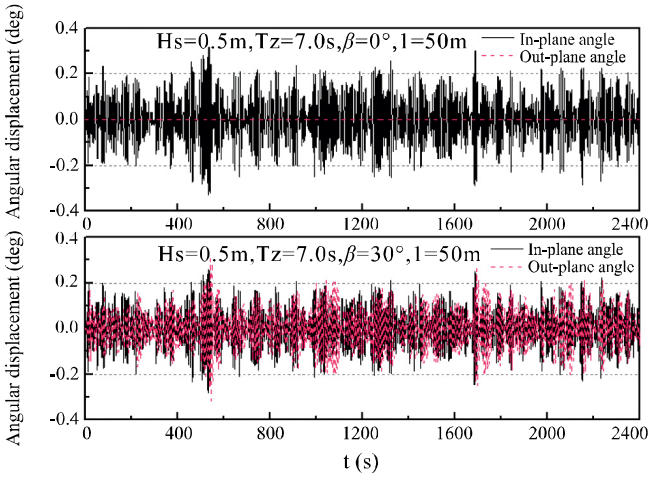

Fig. 11. Angular displacements of the lifted cargo.

$Hs = 0.5m, Tz = 7.0s, l = 50m$

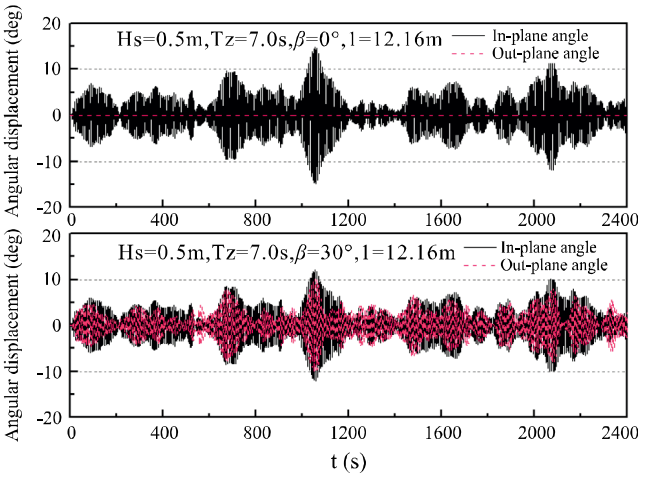

Fig. 12. Angular displacements of the lifted cargo.

$Hs = 0.5m, Tz = 7.0s, l = 12.16m$

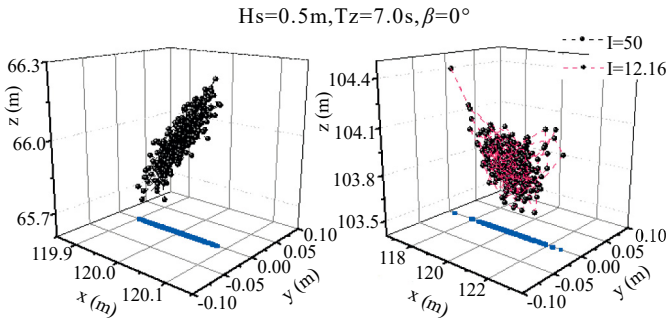

Fig. 13. Trace of the lifted cargo in space.

$Hs = 0.5m, Tz = 7.0s, \beta = 30°$

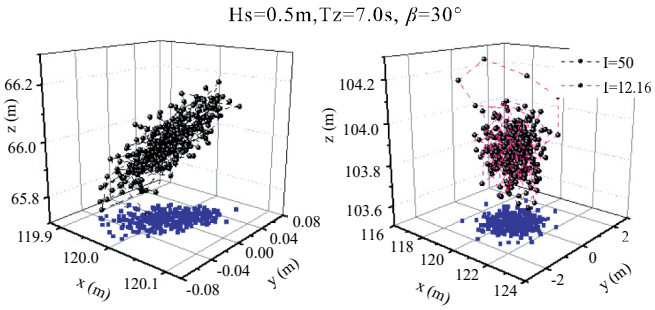

Fig. 14. Trace of the lifted cargo in space.

$Hs = 0.5m, Tz = 7.0s, \beta = 30°$

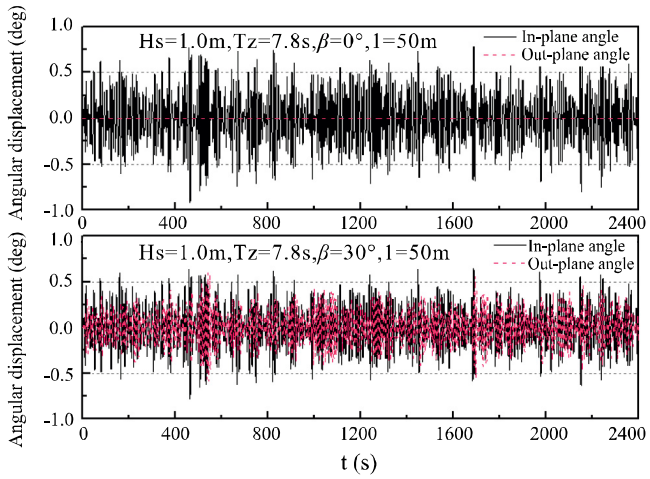

Fig. 15. Angular displacements of the lifted cargo.

$Hs = 1.0m, Tz = 7.8s, l = 50m$

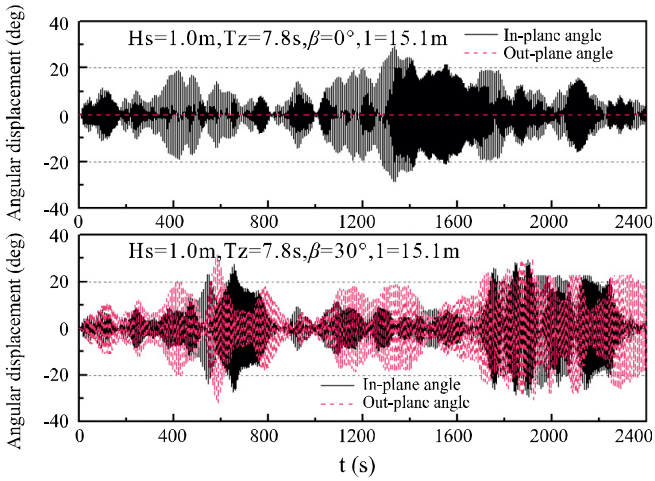

Fig. 16. Angular displacements of the lifted cargo.

$Hs = 1.0m, Tz = 7.8s, l = 15.1m$

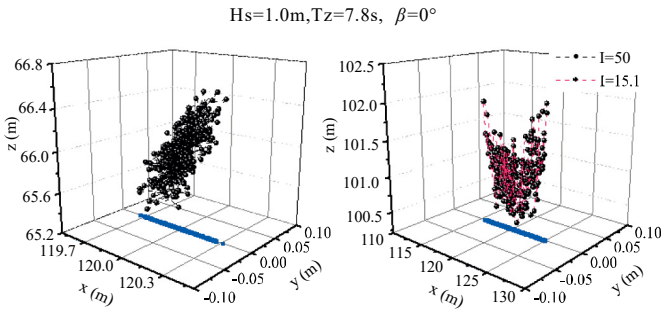

Fig. 17. Trace of the lifted cargo in space.
$Hs = 1.0m, Tz = 7.8s, \beta = 30°$

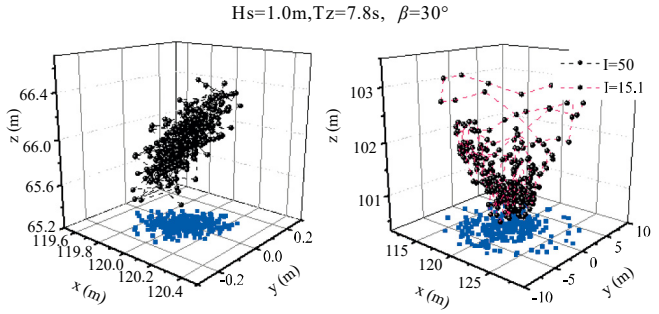

Fig. 18. Trace of the lifted cargo in space.
$Hs = 1.0m, Tz = 7.8s, \beta = 30°$

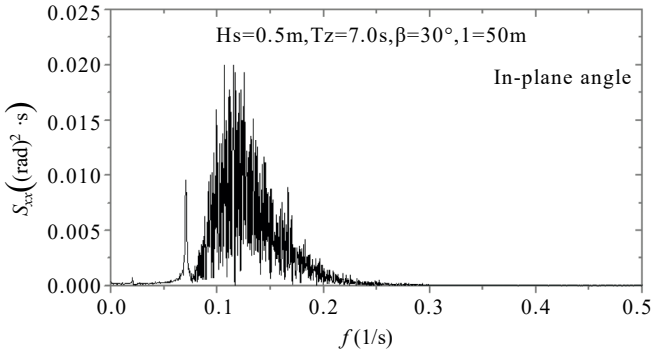

Fig. 19. Amplitude spectrum of in-plane angle
$Hs = 0.5m, Tz = 7.0s, l = 50m$

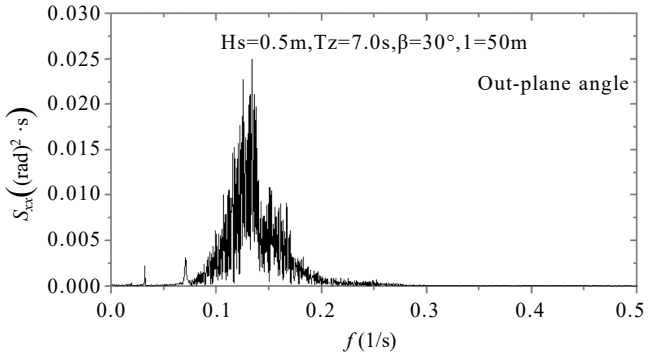

Fig. 20. Amplitude spectrum of out-plane angle.
$Hs = 0.5m, Tz = 7.0s, l = 50m$

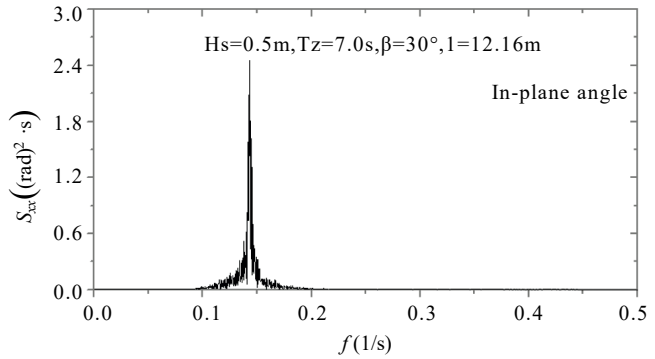

Fig. 21. Amplitude spectrum of in-plane angle.
$Hs = 0.5m, Tz = 7.0s, l = 12.16m$

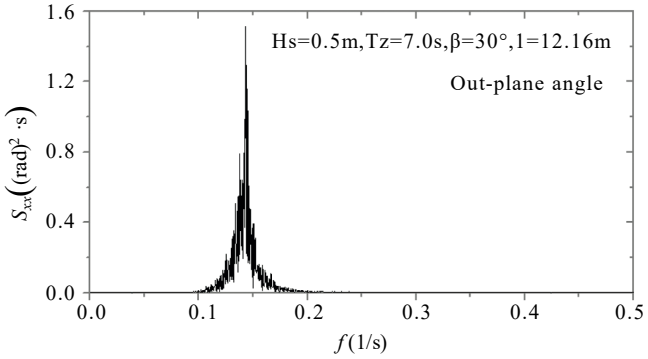

Fig. 22. Amplitude spectrum of out-plane angle.
$Hs = 0.5m, Tz = 7.0s, l = 12.16m$

3.2m at 0.5m wave height and 7.6m at 1.0m wave height.

The displacements of the lifted cargo are small when the difference between the length of the sling and that of the resonance is big enough.

The displacement of the lifted cargo is more affected by the change of wave frequency than that of wave height. In the case of head sea, the horizontal displacement of the lifted cargo is 0.4m when the wave height is 1.0m and the sling length is 50m while it is 0.23m at 0.1m wave height and the sling length is 8.35. There is only a 0.17m difference between the displacements.

Because the horizontal displacement of lifted cargo has reached to meter-scale in sea state II, it is necessary to take measures to reduce displacements of the crane ship in order to ensure the accuracy of the lifting work (e.g. increase a mooring line pre-tension).

(2) Response spectrums of the lifted cargo in sea state II

In the first oblique waves (β=30°), the response spectrums of the lifted cargo with different sling lengths are shown in Fig. 19--Fig. 22. Frequency (f) unit is Hz (1/s) and the amplitude unit

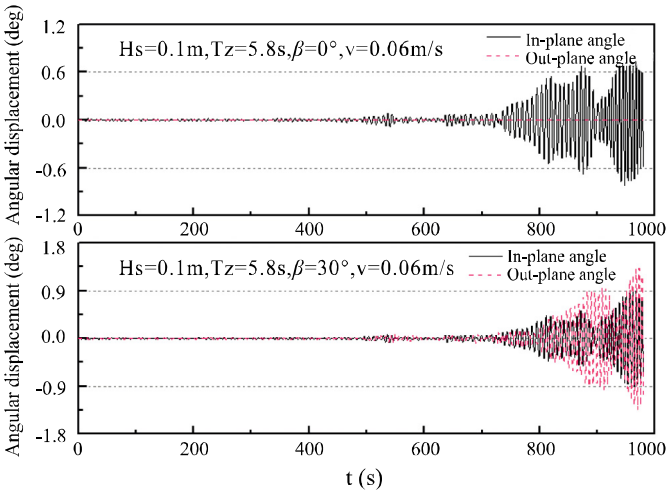

Fig. 23. Angular displacements of the lifted cargo.

$Hs = 0.1m, Tz = 5.8s, v = -0.06m/s$

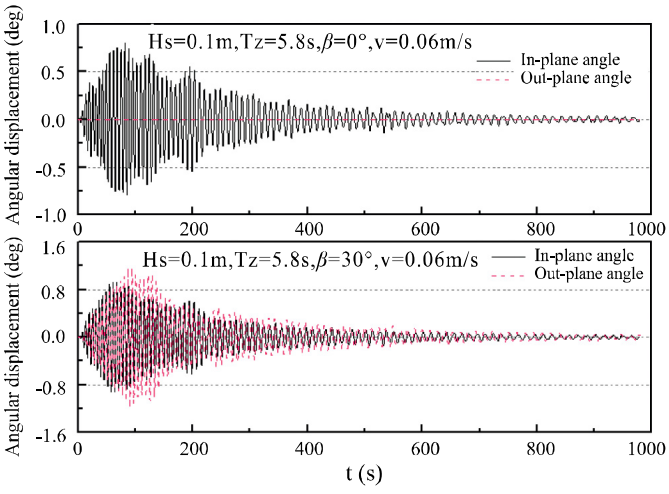

Fig. 24. Angular displacements of the lifted cargo.

$Hs = 0.1m, Tz = 5.8s, v = -0.06m/s$

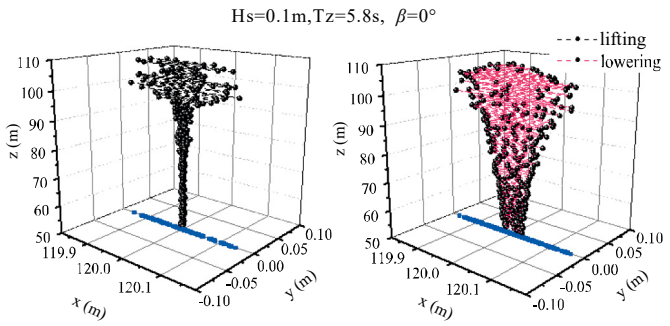

Fig. 25. Trace of the lifted cargo in space.

$Hs = 0.1m, Tz = 5.8s, \beta = 0°$

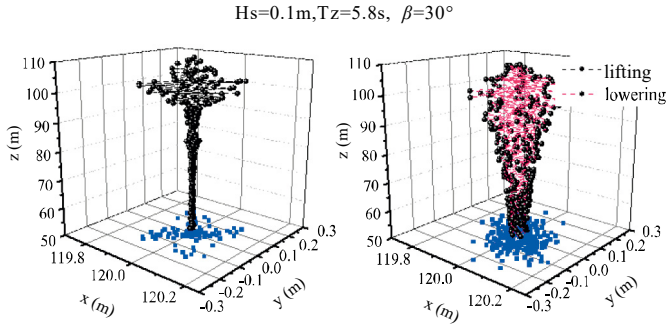

Fig. 26. Trace of the lifted cargo in space.

$Hs = 0.1m, Tz = 5.8s, \beta = 30°$

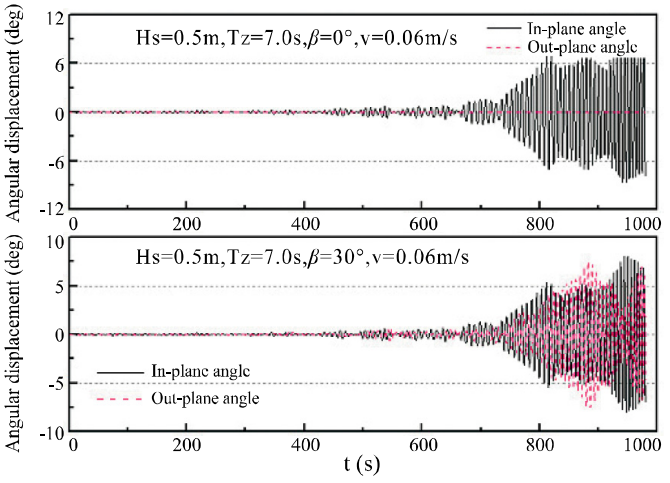

Fig. 27. Angular displacements of the lifted cargo.

$Hs = 0.5m, Tz = 7.0s, v = -0.06m/s$

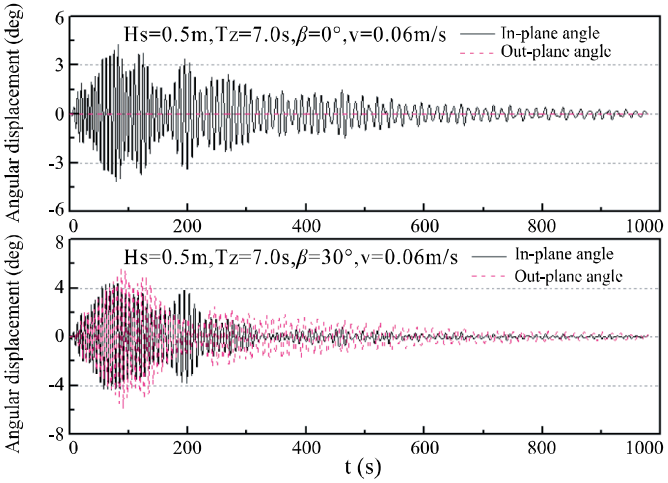

Fig. 28. Angular displacements of the lifted cargo.

$Hs = 0.5m, Tz = 7.0s, v = -0.06m/s$

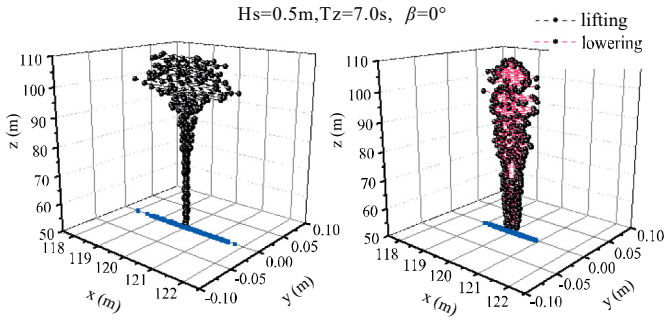

Fig. 29. Trace of the lifted cargo in space.

$Hs = 0.5m, Tz = 7.0s, \beta = 0°$

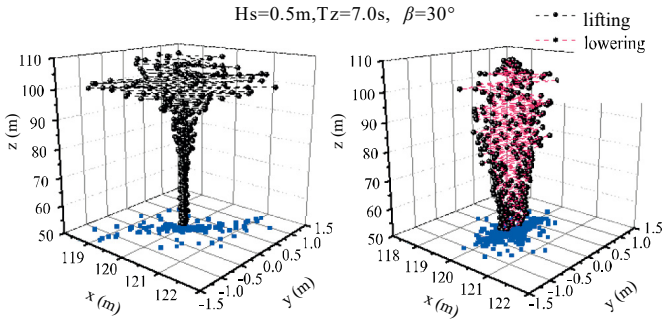

Fig. 30. Trace of the lifted cargo in space.

$Hs = 0.5m, Tz = 7.0s, \beta = 30°$

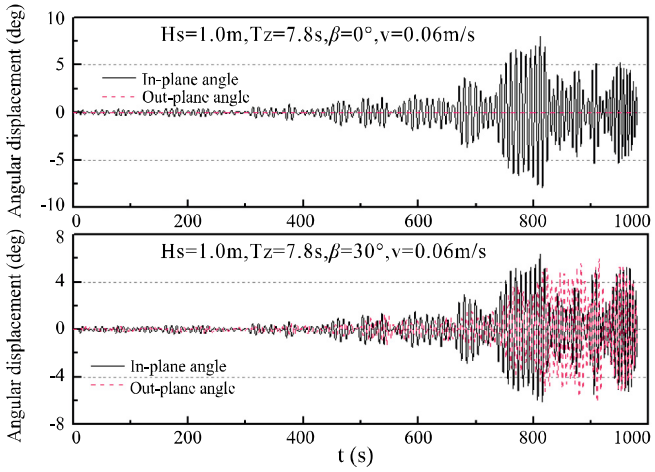

Fig. 31. Angular displacements of the lifted cargo

$Hs = 1.0m, Tz = 7.8s, \beta = 0.06m/s$

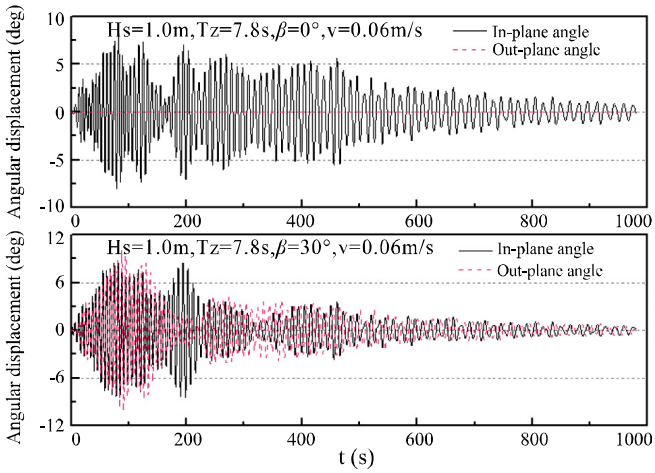

Fig. 32. Angular displacements of the lifted cargo.

$Hs = 1.0m, Tz = 7.8s, v = -0.06m/s$

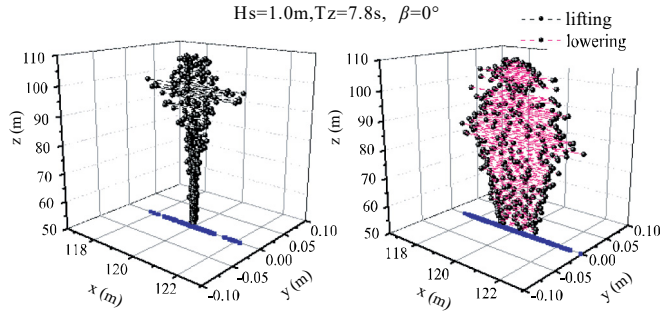

Fig. 33. Trace of the lifted cargo in space.

$Hs = 1.0m, Tz = 7.8s, \beta = 0°$

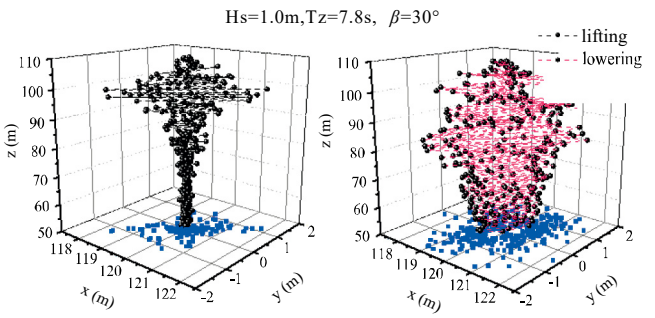

Fig. 34. Trace of the lifted cargo in space.

$Hs = 1.0m, Tz = 7.8s, \beta = 30°$

of self-power spectral density (S_{XX}) is $(\text{rad})^2 \cdot \text{s}$ in these figures. From Fig. 19 to Fig. 22, we can find the response spectrums of the lifted cargo in sea state II shows a wide range of angular displacement frequency when the sling length is 50m and a narrow one when the length of the sling is resonance one(12.16m). And in the latter condition, the energy of the lifting load system is more concentrated and the peak values of the response spectrums of the lifted cargo are more obvious. However, the curves of the response spectrums present obvious nonlinear features. The amplitudes of the angular displacement jump along the curves of the response spectrums, which are the response features of the lifting load system in irregular waves.

(3) Displacements and trace of the lifted cargo in lifting and lowering

In this section, we analyze the displacements and trace of the lifted cargo in lifting and lowering in irregular waves. The calculation parameters in different sea states are shown in Table 16. The calculation results can be seen from Fig. 23 to Fig. 34 and the maximum displacements are shown in Table17.

A. Angular displacements and trace of the lifted cargo in sea state I.
B. Angular displacements and trace of the lifted cargo in sea state II.
C. Angular displacements and trace of the lifted cargo in sea state III.

It can be noticed from Fig. 23-Fig. 34 that traces of the lifted cargo in space diverge over time in lifting the cargo and maximum displacements of the lifted cargo in lifting is less than resonant displacements of the sling length keeping the same. Thus it can be seen that the lifting movement of the cargo suppress the growth of displacements of the lifted cargo. In head sea, when the cargo is lifted, the sling length becomes shorter and shorter until it reaches 14m where the amplitude of the in-put angle of the lifted cargo reaches resonant amplitude which undergoes a gradual increase until the sling length shortens to 6m. At that point, the amplitude starts to diminish.

The same is also found in lowering the cargo: the in-put angle amplitude of the lowered cargo increases with the change of the sling length until it reaches a certain point. At that point, the amplitude starts to diminish. The only difference is that in lowering the cargo, the process takes more time. Thus it can be seen that in lowering the cargo, displacements of the lifted cargo gradually increase to resonant amplitude and then decrease with the change of the sling length. Maximum displacements of the lifted cargo in lowering the cargo are also less than resonant displacements of the sling length keeping the same.

It can be observed from Fig. 23-Fig. 34 that the lifting load system also undergoes beat vibration in irregular waves as well as in regular waves, but the beat vibration in irregular waves is less obvious than in regular waves

VI. CONCLUSION

The time domain model of a crane ship is applied and the coupled motion between a crane ship and its lifting load system is performed in this paper. The motion equations of the lifting load system are derived from Lagrange equations. The motion analysis of a crane ship is based on 3D potential flow theory. Choosing irregular waves as the calculation sea states, time domain simulations of a crane ship and its lifting load system are performed related to different parameters. Some results are obtained such as the displacements of a crane ship, the angular displacements of lifted cargo and its trace in space.

(1) Whether in regular or irregular waves, when working in the head sea, the motion of the crane ship is single degree of freedom, the in-plane and out-plane angle coupling effect is not obvious. However, in oblique waves, especially in irregular waves, the coupling effect is obvious, which shows nonlinear motion features of the lifted cargo.
(2) The resonance length of the sling increases with the increase of the wave period. At resonant region, the amplitudes of in-plane angle and out-plane angle of the lifted cargo increase significantly. The displacement of the lifted cargo is more affected by the change of wave frequency than that of wave height.
(3) In lifting and lowering, the maximum resonant responses of the lifted cargo are less than that in constant sling length. In lifting, the responses of the lifted cargo are amplified rapidly in resonant region. Relatively, the lifting load system must take more time to depart from its resonant region in lowering.
(4) In irregular sea waves, the curves of amplitude-frequency characteristics present strongly nonlinear features, but its peak value is obvious, the frequency of which is close to that of sea waves. The range of motion response frequency of the lifted cargo becomes narrow when its motion response nears resonant one.

REFERENCES

Al-Sweiti, Y. M. and D. Söffker (2007). Planar cargo control of elastic ship cranes with the "Maryland rigging" system. Journal of vibration and Control 13(3), 241-267.

Balachandran, B., Y.-Y. Li and C.-C. Fang (1999). A mechanical filter concept for control of non-linear crane load oscillations. Journal of Sound and Vibration 228(3), 651–682.

Cha, J. H., M.- I. Roh and K. Y. Lee (2010). Dynamic response simulation of a heavy cargo suspended by a floating crane based on multibody system dynamics. Ocean Engineering 37(14-15), 1273-1291.

Chen, L., C. Zhang and X. Y. Zhang (2011). The response of large crane ship to waves. Shanghai Ship and Shipping Research Institute 34 (2), 299-102.

Chin, C., A. H. Nayfeh and E. Abdel-Rahman (2001). Nonlinear dynamics of a boom crane. Journal of Vibration and Control 7(2), 199-220.

Chin,C. M., A. H. Nayfeh and Dean T. Mook (2001). Dynamics and control of ship-mounted cranes. Journal of Vibration and Control September 7(6), 891-904.

Clauss, G. and T. Riekert (1992). Influence of load motion control on the operational limitations of large crane vessels in severe environment. In: Proceedings International Conference on Behaviour of Offshore Structures, BPP Technical Services, 1112–1125.

Cummins ,W.E. (1962). The Impulse Response Function and Ship Motions. Symposium on Ship Theory.

D. X., Li (2002). Advanced structural dynamics. science press.

Dai, Y.H. and W. Y. Duan (2008). Potential theory of ship in waves. M. National Defence Industry Press.

Ellermann, K., M. Markiewicz and E. Kreuzer (2002). Nonlinear Dynamics of Floating Cranes. Nonlinear Dynamics 27(2), 107-183.

Harnett, M. (2000). The application of a spectral response model to fixed offshore structures. Journal Compeers and Structures 78, 355-364.

Henry,R. J., Z. N. Masoud, A.H. Nayfeh and D.T. Mook (2001). Cargo pendulation reduction on ship-mounted cranes via boom-luff angle actuation. Journal of Vibration and Control 7(8), 1253-1264.

Hong, K.-S. and Q. H. Ngo (2012). Dynamics of the container crane on a mobile harbor. Ocean Engineering 53, 16-24.

Hu,Y. J., D. X. Wen and X. L. Wang (2012). Swing analysis of suspended load system for crane ship of transporting and lifting girders. Journal of Sys-

tem Simulation 24(7),1501-1509.

Journée, J. M. J. (1993). Hydromechanic coefficients for calculation time domain motions of cutter suction dredgers by cummins equations. Report 968, Delft University of Technology, The Netherlands.

Kral, R., E. Kreuzer and C. Wilmers (1995). Nonlinear oscillations of a crane ship. Proceedings of the 3rd International Conference on Industrial and Applied Mathematics, Suppl. 4, 5-8.

Masoud ,Z. N., A. H. Nayfeh and D. T. Mook (2004). Cargo pendulation reduction of ship-mounted cranes. Nonlinear Dynamics 35(3), 299-311.

Ngo, Q. H. and K.-S. Hong (2012). Sliding-mode antisway control of an offshore container crane. IEEE-ASME Transactions on Mechatronics 17(2), 201-209.

Ren, H. L., X. Wang, Y. J. Hu and C. G. Li (2008). Dynamic response analysis of a moored crane-ship with a flexible boom. Journal of Zhejiang University Science A. 9(1), 26-31.

Schellin ,T. E., T. Jiang and S. D. Sharma (1991). Crane ship response to wave groups. Journal of Offshore Mechanics and Arctic Engineering 113(3), 211-218.

Tang, Y.G., R.Y. Zhang, N. Cheng and J. R. Zhao (2009). Analysis of snap tension of deep water mooring with lumped mass method. Journal of Tianjin university Science and Technology 42(8), 695-701.

Todd, M. D., S. T. Vohra and F. Leban (1997). Dynamical measurements of ship crane load pendulation. Oceans 1997 MTS/IEEE Conference Proceedings. 2, 1230-1236.

Wang, X., X. You and Y. Hu (2010). Cargo pendulation analysis of moored crane ship under regular waves. China Mechanical Engineering 21(9), 1077-1082.

Wu, X. H, L. W. Zhang and R. K. Wang (1988). Controllability and Seakeeping of a Ship. China Communication Press.

Xiao, Y. (2006). Nonlinear analysis of time domain for mooring system. Journal Dalian University of Technology.

Zhang, X. and T.S. Wang (2007). Computational Dynamics. Tsinghua University Press.

.